The Effective Temperatures and Physical Properties of Red Supergiants: The Effects of Metallicity

MASSACHUSETTS INSTITUTE OF TECHNOLOGY
JAN 3 0 2006
LIBRARIES

by

Emily Moreau Levesque

Submitted to the Department of Physics
in partial fulfillment of the requirements for the degree of

Bachelor of Science in Physics

at the

MASSACHUSETTS INSTITUTE OF TECHNOLOGY
[June 2006]
December 2005

©Emily Levesque, 2006. All rights reserved.

The author hereby grants to MIT permission to reproduce and to distribute publicly paper and electronic copies of this thesis document in whole or in part in any medium now known or hereafter created.

ARCHIVES

Author .....
Department of Physics
December 13, 2005

Certified by .....
Adam Burgasser
Assistant Professor, Department of Physics
Thesis Supervisor

Certified by .....
Philip Massey
Research Scientist, Lowell Observatory
Thesis Supervisor

Accepted by .....
Professor David E. Pritchard
Senior Thesis Coordinator, Department of Physics

The Effective Temperatures and Physical Properties of Red Supergiants: The Effects of Metallicity

by

Emily Moreau Levesque

Submitted to the Department of Physics
on December 13, 2005, in partial fulfillment of the
requirements for the degree of
Bachelor of Science in Physics

Abstract

In this thesis I use moderate-resolution optical spectrophotometry and the new MARCS stellar atmosphere models to determine the effective temperatures of 74 red supergiants (RSGs) in our galaxy, 39 RSGs in the Small Magellanic Cloud (SMC), and 36 RSGs in the Large Magellanic Cloud (LMC). The new effective temperature scales derived from these data are significantly warmer than those in the literature. The known distances of these stars allows a critical comparsion with modern stellar evolutionary tracks, and the newly derived temperatures and bolometric corrections generally give much better agreement with predictions of massive star evolution for all three of these galaxies. I also use these new temperature scales to demonstrate a correlation between galactic metallicity and the average spectral subtype of a galaxy's RSG population.

Research contained in this thesis has been published in part by the Astrophysical Journal, v. 628, p. 973

Research contained in this thesis has been submitted to the Astrophysical Journal for publication in a future volume.

Thesis Supervisor: Adam Burgasser
Title: Assistant Professor, Department of Physics

Thesis Supervisor: Philip Massey
Title: Research Scientist, Lowell Observatory

Acknowledgments

I would like to thank Dr. Philip Massey of Lowell Observatory for his exceptional guidance and encouragement throughout the duration of this research, as well as the National Science Foundation's Research Experience for Undergraduates program at Northern Arizona University (NSF Grant AST 99-88007). Thanks must also be extended to Dr. Adam Burgasser, who provided excellent advice and supervision during the writing of this thesis.

This research would not have been possible without collaborators Knut Olsen, Bertrand Plez, Eric Josselin, Andre Maeder, Georges Meynet, and Geoff Clayton. This work was supported in part by NSF grant AST 00-093060. In conclusion, I would like to thank the Department of Physics at MIT for supporting this research and all of my academic endeavors as a department undergraduate.

Contents

List of Figures

List of Tables

Chapter 1

Introduction

Red supergiants (RSGs) are an important but poorly characterized stage in the evolution of massive stars. While a massive star may spend only 10% of its life in this stage (as He-burning stars), it is a critical mass-loss period for high-mass stars progressing to the Wolf-Rayet stage, as well as a precursor to the supernova explosion that marks the end of the star's life. RSGs are also dominant sources of near infrared (NIR) light in star clusters and galaxies (Östlin & Mouhcine, 2005). Additionally, the dust produced in the RSG phase contributes to the grains making up the diffuse interstellar medium.

Until recently, these stars were poorly characterized by evolutionary tracks (Massey, 2003, and Massey & Olsen, 2003). Stellar evolution models have long failed to produce RSGs that are as cool or as luminous as those observed. Such a discrepancy is not surprising, given the tremendous challenge RSGs have presented to evolutionary predictions.

RSG atmospheric properties are uncertain because of possible deficiencies in our knowledge of molecular opacities. The atmospheres of these stars are highly extended and hydrodynamic, with stellar winds resulting in significant mass-loss. In addition, the velocities of the convective layers are nearly sonic, and even supersonic in the atmospheric layers, giving rise to shocks (Freytag et al. 2002). These shocks invalidate mixing-length assumptions, making the star's photosphere asymmetric and its radius poorly defined, as demonstrated by high angular resolution observations of Betelgeuse

(Young et al. 2000). By contrast, evolution models are forced to adopt a plane-parallel static geometry.

While considering these challenges, we must, however, recognize that the "observed" location of RSGs in the Hertzsprung-Russell (H-R) diagram (plotting temperature against luminosity) is also highly uncertain, since this location requires a sound knowledge of a star's temperature at its surface (as approximated by optical depth), otherwise known as its effective temperature (T_{eff}). For stars this cool (roughly 3000 - 4500 K), the magnitude corrections required to yield the bolometric magnitude from the absolute magnitude (magnitude measured at 10 pc), commonly known as bolometric corrections (BCs) are given by

$$M_{bol} = M_{passband} - BC_{passband} \tag{1.1}$$

are quite significant (-4 to -1 magnitudes in V), and are also a steep function of T_{eff}. This makes an accurate effective temperature scale very important, since even a 10 % error in T_{eff} yields a factor of 2 error in bolometric luminosity as described by Massey & Olsen (2003).

There are not enough nearby RSGs to use interferometric data for determination of an effective temperature scale. Previous scales have used broadband colors to assign temperatures based on the few RSGs with measured diameters (Lee 1970, following Johnson 1964, 1966), or on observed BCs (from infrared measurements) combined with the assumption of a blackbody distribution for the continuum (Flower 1975, 1977). White & Wing (1978) employed a novel scheme involving an eight color narrowband filter set, which was fit by a blackbody curve and iteratively corrected to determine uncontaminated continua. There is, however, significant degeneracy between changes in the effective temperature of the model and changes in the applied reddening. Here the term "reddening" refers to the scattering of shorter (bluer) wavelengths by interstellar dust particles along the observer's line of sight. This is especially important for RSGs as they can be heavily reddened due to their large distances.

An alternative approach would be to make use of the TiO molecular bands that dominate the optical spectra of M-type stars. However, atmospheric models have not always included accurate opacities, especially for molecular transitions.

The new generation of MARCS models (Gustafsson et al. 1975; Plez et al. 1992) now includes a much-improved treatment of molecular opacity (see Plez 2003; Gustaffson et al. 2003). These models can be used to make a far more robust determination of T_{eff} and reddening, by comparison to absolute spectrophotometry of RSGs. Use of both continuum fluxes and the strengths of the TiO bands effectively removes the previous degeneracy for both K and M stars. Since TiO band strengths are used to determine RSG spectral types, the MARCS models are also the key to the first definitive connection between spectral type and T_{eff}.

The strengths of the TiO bands are dependent on T_{eff}, but it is expected that there is also a dependence on atmospheric TiO abundance, which varies according to the metallicity of the RSGs' environment. A direct correlation between TiO abundance and spectral subtype has been suggested by Massey & Olsen (2003) - changes in the abundance of TiO may directly yield changes in spectral subtype for a given T_{eff}. It is also suggested that metallicity may affect the time a massive star spends in the RSG stage (Maeder et al. 1980). As described by Conti (1976), the loss of a massive star's H-rich outer laters as it evolves into a Wolf-Rayet star (a hot, luminous massive star with its helium core exposed as a result of this mass loss) is driven by radiation pressure acting through highly ionized metal lines. This suggests that the mass-loss rate will be greater at higher metallicities for a given luminosity (Massey, 1998).

The Magellanic Clouds (MCs) have lower metallicities than our own galaxy: $z = 0.002$ for the Small Magellanic Cloud (SMC) and $z = 0.008$ for the Large Magellanic Cloud (LMC), as compared to $z = 0.020$ in the Milky Way (here z is defined to be the proportion of elements heavier than H and He present). The distribution of RSG spectral subtypes in the MCs is also considerably earlier than in the Milky Way - the average spectral type is K5-K7 I in the SMC and M1 I in the LMC, as compared to M2 I in the Milky Way (Massey & Olsen 2003). These varying distributions may be at least partially attributable to variations in metallicity.

In this thesis I present spectrophotometry of 149 K- and M-stype RSGs: 74 in the Milky Way, 39 in the SMC, and 36 in the LMC. Fitting the spectral energy distributions of these stars to MARCS models of the appropriate metallicity, I have determined the effective temperatures of these stars and constructed new T_{eff} scales for RSGs in each galaxy. Most of the Galactic stars are members of associations and clusters with known distances, and the distances to the LMC and SMC are well-known, which allows me to place the stars on the H-R diagram for comparison with the latest generation of stellar evolutionary models. I also compare the three temperature scales to examine the possible correlation between metallicity and average spectral subtype.

Future work will apply these techiques to eight red supergiants in M31, using data obtained at the MMT (observations planned for September 2005 were cancelled following delays at the observatory). This comparison to a galaxy of higher metallicity ($z = 0.04$) will allow further examination of the relationship between metallicity and spectral subtype and the effects of metallicity on the evolution of RSGs.

Chapter 2

Observations

2.1 Galactic Observations

Optical spectrophotometric data were obtained for the RSGs are listed in Table 1. The sample was selected in order to cover the full range of spectral subtypes from K1 to M5. These stars are all members of OB assocations and clusters with known distances (Humphreys 1987; Garmany & Stencel 1992), and the sample is supplemented with spectral standards (Morgan & Keenan, 1973) to help refine spectral classification. In Table 2 I give the distances from several sources (when possible) for each OB association or cluster used in our sample; in general the agreement is within a few tenths of a magnitude.

2.1.1 Spectrophotometry

The data were obtained during three seperate observing runs: two with the Kitt Peak National Observatory 2.1-m telescope and GoldCam spectrograph (2004 March 17-24 and May 28 - June 1) and one with the Cerro Tololo Inter-American Observatory 1.5-m telescope and Cassegrain CCD spectrometer (2004 March 7-12). Similar resolutions and wavelength coverage were obtained in all three runs. Detailed information on the observing parameters is given in Table 3.

The Kitt Peak observations were taken under sporadically cloudy conditions in

March by Dr. Philip Massey. May/June data was obtained by Dr. Philip Massey and myself, and all nights were photometric. Before observing each object, the spectrograph was manually rotated so that the slit was aligned with the parallactic angle, enabling collection of accurate photometric data. We aimed for a signal-to-noise ratio of 50 per spectral resolution element (4 pixels) at the bluest end of the spectrum (4100 Å), with care being taken not to saturate the detector at the reddest end of the spectrum (9000 Å). Slit widths were 170 μm in the blue (3200 - 6000 Å) and 250 μm in the red (5000 - 9000 Å). For the brightest stars ($V < 6$), we employed 5.0 or 7.5 mag neutral density filters. Observations of a flat-field quartz lamp pointed at the CCD ("projector flats") were obtained both with and without these filters in order to correct for the wavelength-dependent transmission of these "neutral" filters. Throughout each night we also observed a set of spectrophotometric standards. The seeing for these observations was 1."2 - 3", with a typical value of 2". Exposures of both dome flats (observations of a uniformly lit white screen inside the telescope dome)and projector flats were obtained at the beginning of each night; for the red nights, we also obtained projector flats throughout the night to monitor any shifting of the interference fringes visible at longer wavelengths. Wavelength calibration exposures of a He-Ne-Ar lamp were obtained at the beginning and end of each night.

Observations at Cerro Tololo were made by Dr. Knut Olsen. At the 1.5-meter it was not practical to always observe at the parallactic angle; instead, each star was observed with a single exposure through a very wide slit (for good relative fluxes), followed by a series of shorter exposures obtained through a narrow slit (for good resolution). Narrow slit widths were 270 μm in the blue (3500 - 5200 Å) and 200 μ in the "orange" (5000 - 7500 Å) and red (6300 - 9000 Å). Projector flats were obtained for all wavelength regions through both the wide and narrow slots. The exposures were typically obtained in conjunction with a wavelength calibration exposure. Observations of spectrophotometric standards were observed throughout the night (the sources of the spectrophotometric standards are given in Table 1.)

2.1.2 Data Reduction

We reduced the data using Image Reducation and Analysis Facility (IRAF) [1] packages CCDRED, KPNOSLIT, and CTIOSLIT. We used dome flats to correct for pixel-to-pixel response variations ("flatten") for the blue Kitt Peak data and projector lamp flats to flatten the red Kitt Peak data and the CTIO data. We found that the only shift in the fringe pattern in the red occurred during the 30 minutes following a refill of the CCD dewar with liquid nitrogen. After that the fringe pattern was stable, so we simply combined the projector flats. The spectra were all extracted using an optimal extraction algorithm. In a few cases the wide-slit observations included the presence of an additional star in the extraction aperture. To eliminate these stars, and to ensure accurate fluxes for the spectrophotometric data, the narrow slit width observations were combined and divided into the wide-slit observations.

The observations of spectrophotometric standards were used to creative sensitivity functions; typically a grey shift was applied to each night's data, and the resulting scatter was 0.02 mag. In addition, the different wavelength regions were grayshifted to agree in the regions of overlap.

2.2 Extragalactic Observations

The observed RSGs are listed in Table 1. The sample was selected to cover the full range of spectral subtypes in both of the Clouds - from K0-1 to M4 for the SMC, and K1 through M4 for the LMC.

2.2.1 Spectrophotometry

The spectrophotometry was obtained by Dr. Philip Massey and myself with the R-C Spectrograph on the CTIO Blanco 4-meter telescope (2004 November 23-25, December 1-2,4), using the Blue Air Schmidt camera and Loral 3K CCD. Detailed

[1] IRAF is distributed by the National Optical Astronomy Observatories, which is operated by the Association of Universities for Research in Astronomy (AURA), Inc., under cooperative agreement with the National Science Foundation.

information on the observing parameters is given in Table 3.

We took the data under conditions ranging from moderate cirrus to photometric with a typical seeing of 1."2 - 2". We took exposures of both dome and projector flats at the beginning of each night, using the projector flats for flat-fielding, and wavelength calibration exposures of a He-Ne-Ar lamp at the beginning and end of SMC and LMC observations. We also observed spectrophotometric standards throughout the night, including several Galactic spectral standards in common with the Galactic observations. All observations were made with the spectrograph slit oriented near the parallactic angle.

2.2.2 Data Reduction

We reduced the data using IRAF packages CCDRED and CTIOSLIT. The spectra were all extracted using an optimal-extraction algorithm. We used the spectrophotometric standards to create sensitivity functions; typically a grey shift was applied to each night's data and the resulting scatter was 0.01-0.02 mag. The standards bracketed the range of airmasses for which the program objects were observed, and standard values were assumed for the extinction.

Given the good agreement of the standard star observations, we were surprised to find that the Galactic RSGs observed in common with those from Levesque et al. (2005) differed quite significantly in the near ultra-violet (NUV), particularly below 3800Å. The spectrophotometric standards agreed very well in this region, but the same disagreement was seen when the new data was compared to both the Kitt Peak and CTIO 1.5-m telescope data from Levesque et al. (2005). We determined that the problem was inherent to the data rather than the reduction techniques. The new data all had extra flux in the NUV, a problem that was eventually correlated with color: the reddest RSGs had the largest discrepancy. The excess NUV flux displayed unexpected structure, in particular at 3810Åwhere a feature was present that strongly resembled the telluric A-band at 7620Å(twice the wavelength!) It was concluded that the flux at these NUV wavelengths was being affected by the flux at twice the wavelength. We had been observing with a first-order grating in the blue,

which ruled out the order-seperation problems typical when a blocking filter is not used. By subtracting the spectrophotometry obtained in the Galactic observations from the CTIO data, and comparing this subtraction to the counts in the red, we established that there was a small percent of 2λ light contaminating the observations. The problem is only noticeably in observations of extremely red stars such as RSGs. Tests by Knut Olsen and Philip Massey in March of 2005 using the comparison arcs and various blocking filters established beyond any doubt that this 632 l mm^{-1} grating also acts as a 316 l mm^{-1} grating, albeit at a low level. Another replica of this grating has been in use for many years with the Kitt Peak 4-m RC spectrograph (KPC-007). After this discovery, Di Harmer kindly conducted a similar test with it and found that it suffers from the same problem. We determined an empirical correction factor, which amounted to several percent of the 2λ count rate, and applied that to all of our data. The spectrophotometric standards yielded the identical solutions. The correction is significant (greater than a few percent) only below 4000Å. So as to not compromise the results of the present study, analysis was restricted only to data with wavelength greater than 4100Å.

2.3 Spectral Features of Red Supergiants

The spectra of a K-type and an M-type red supergiant can be found in Figure 1. K-type RSG spectral energy distributions (SEDs) show a strong G band and shallow TiO absorption features. M-type SEDs are dominated by multiple deep TiO bands and the Ca I and Ca II lines around

Chapter 3

Analysis

3.1 Reclassification of Spectral Type

I reclassified each of the stars by visually comparing each spectrum to the spectral standards. In order to avoid questions of normalizing these rich and complicated spectra (with uncertain continuum levels), this comparison was done on a log flux scale. Since many of these stars can be variable in spectral type (surface pulsations and outbursts vary the T_{eff} and hence the spectral type), it was unsurprising that a few spectral standards had to be reclassified for consistency. The classification was based on the depths of the TiO bands, which are increasingly stronger with later spectral type (and, as demonstrated in the following section, with decreasing temperature!) Initially, I attempted to classify the early and mid-K supergiants based solely on the strength of the G-band, but this feature was found to be extremely insensitive to temperature and progressing spectral type among the standards. I found instead that the 5167Å TiO line was a good basis for comparison, present even in the early K stars. For consistency, the same method of fitting - comparison of the TiO line depths in the central region of the spectrum - was used for spectral reclassification and determination of T_{eff}. A good fit was determined both by agreement of TiO line depths and shape of the SED, with particular attention paid to the G-band and the redder wavelengths (see section 3.5). The revised spectral types are listed in Table 4.

3.2 Model Fitting: Effective Temperatures and Reddenings

I compared the observed spectral energy distribution (SED) of each star to a series of MARCS stellar atmosphere models. The models used in these comparisons ranged from 3000 to 4300K in increments of 100K for the Galactic-metallicity models, and from 3000 to 4600K in increments of 100K for the LMC- and SMC-metallicity models, with log g (in cm/s^2, where log g of the sun is 4.2) ranging from +1.0 to −1.0 in increments of 0.5 dex. The models were linearly interpolated to produce additional models at steps of 25 K. The choice of surface gravity was derived iteratively; I would first adopt the log $g = -0.5$ models for all of the fits, as this surface gravity was generally what was expected with the old T_{eff} scale's placement of RSGs in the H-R diagram. However, the new temperatures shifted this placement, so the fits were reevaluated using log $g = 0.0$ models, as this was more consistent with the revised locations, and then reevaluated iteratively until a satisfactory log g was chosen for each star - the results typically converged quickly. The effective temperatures remained unchanged with the use of higher surface gravities, but the values of the color excess $E(B-V)$ increased slightly.

I wrote an Interactive Data Language (IDL) program designed to plot different models against each observed SED. The SEDs were plotted in log units of flux to facilitate comparisons of line depths without the uncertain process of normalization. The IDL program allows adjustment of the model's temperature and surface gravity, as well as how much reddening is applied to the chosen model. While the program initially dereddened the observed spectra, it was later decided that reddening of the models was a more sound approach. In making the fits, I reddened each model using a Cardelli et al. (1989) reddening law with the standard ratio of total-to-selective extinction $R_V = 3.1$. The initial guess for $E(B-V)$ was based on the average value for the star's cluster or association ($E(B-V)_{cluster}$) from Table 2. The temperature was determined from the relative strengths of the TiO bands, which remain unaffected by the flux-independent scattering effects of reddening. $E(B-V)$ was then adjusted

to produce the best fit to the continuum. Using the same standard that was applied to spectral classification of these stars, a good model fit was determined by agreement of TiO line depths and the overall shape of the SED. In Figure B-2 I show a sample of spectra and fits from all three galaxies, covering a range of spectral types.

Ca I and Ca II line strengths in the MARCS models were found to be too strong to use for fitting these stars (Levesque et al. 2005), but otherwise the models agreed well with both the fluxes and spectral features of the observed SEDs. Due to questions concerning the possibility of circumstellar reddening around RSGs (see section 3.5) and grating problems (see section 2.2.2), I cannot yet draw detailed conclusions regarding the goodness of the model fits in the NUV.

I list the new T_{eff}s in Table 4. In general, the data could be matched very well by the models, both in line strength and continuum shape. The effective temperatures of the late-K and M supergiants have been determined to a precision of approximately 50 K. Given the weakness of the 5100Å line at early-K types and poor G band sensitivity to changes in temperature, T_{eff}s for the early and mid-K stars have been obtained to a precision of approximately 100 K. The interstellar exctinction (A_V) values are determined to a precision of about 0.15 mag, where $A_V = E(B-V) \times R_V$.

3.3 The New Effective Temperature Scales and Effects of Metallicity

The new T_{eff} scale for each galaxy is listed in Table 5, where I include the mean T_{eff}, the number of stars, and the standard deviation of the mean (σ_μ) for each spectral subtype. I compare the Galactic scale to that of Humphreys & McElroy (1984) and Massey & Olsen (2003) in Figure B-3. Both of the latter are "averages" from the literature. Figure B-3 shows that the new scale agrees well for the K supergiants but is progressively warmer than past scales for later spectral types, with the differences amounting to 400 K by the latest M supergiants (M5 I). The overall progression of the temperature with later spectral type is more gradual than in past studies.

The T_{eff} scales of the three galaxies are illustrated in Figure B-4. In general the effective temperature scale for RSGs in the LMC is about 50 K cooler in the LMC than in the Milky Way, and about 150 K cooler in the SMC than in the Milky Way. A star with a T_{eff} of 3700 K would be an M2 I star in the Milky Way, an M1-1.5 I in the LMC, and a K7-M0 in the SMC. Changes in metallicity between these three galaxies indicate changes in the abundance of metals such as Ti and O. A decreased abundance would yield weaker TiO absorption lines for a star of the same effective temperature since there is less TiO available in the star's atmosphere to begin with. This in turn would yield an earlier spectral subtype. Thus, the difference in spectral subtype due to the decreased abundance of TiO can explain the change in the average distribution of RSG spectral subtypes across these three galaxies. If this picture is accurate, then this trend should also apply as metallicity increases for galaxies such as M31 (z=0.036) (Massey 2003), and I plan to extend this work to M31 with observations at the Multiple Mirror Telescope at Mt. Hopkins next summer.

3.4 Comparisons to Evolutionary Models

In order to compare these stars to the evolutionary models, the absolute V luminosities must be converted to bolometric luminosities using Eq. 1.1. The bolometric magnitudes (M_{bol}s) for each star with a known distance are listed in Table 4.

In Table 5 I have included the BCs to the V band corresponding to the new T_{eff} scale; these values are the linear interpolations of the BCs from the MARCS models given in Table 6. The values given are for $\log g = 0.0$, but there is little change with surface gravity (<0.05 mag over 0.5 dex in $\log g$ for $3500 \leq T_{eff} \leq 4300$ K). Note that I have referenced the BCs to the system advocated by Bessell et al. (1998), i.e., that the Sun has a BC of -0.07 mag.

In determining the bolomtric luminosities, the models were used to compute the BC at V as a function of T_{eff} for each galaxy (in magnitudes):

$z = 0.02$ (Milky Way)

$$\mathrm{BC}_V = -298.954+217.532(T_{\rm eff}/1000K)-53.1400(T_{\rm eff}/1000K)^2+4.34602(T_{\rm eff}/1000K)^3$$

$z = 0.008$ (LMC)

$$\mathrm{BC}_V = -121.364+78.41064(T_{\rm eff}/1000K)-16.8979(T_{\rm eff}/1000K)^2+1.20674(T_{\rm eff}/1000K)^3$$

$z = 0.002$ (SMC)

$$\mathrm{BC}_V = -120.102+82.3070(T_{\rm eff}/1000K)-19.0865(T_{\rm eff}/1000K)^2+1.48927(T_{\rm eff}/1000K)^3$$

In Figure B-5 (upper left) I show the solar metallicity evolutionary tracks of Meynet & Maeder (2003) compared to the location of the Galactic RSGs taken from Humphreys (1978) using the T_{eff}s and BCs of Humphreys & McElroy (1984). The disagreement is not as bad as that shown by Massey (2003), as the new tracks extend further to the right at higher luminosities than did the old tracks of Schaller et al. (1992). Nevertheless, it is clear that there are significant differences between theory and "observation". In Figure B-45 (upper right) I compare these same evolutionary tracks to our observed Galactic RSGs, using the new T_{eff}s and M_{bol}s found by using the MARCS models. I have marked, with filled circles, five stars for which the K-band data suggest that our M_{bol} values are too luminous (the K-band M_{bol}s for these five stars are given in Table 4), and in Figure B-45 (lower left) the stars' locations are shown based on K-band data, where the BC at K is given in magnitudes by:

$z = 0.02$ (Milky Way)

$$\mathrm{BC}_K = 5.571 - 0.7589(T_{\rm eff}/1000K)$$

$z = 0.008$ (LMC)

$$\mathrm{BC}_K = 5.502 - 0.7392(T_{\rm eff}/1000K)$$

$z = 0.002$ (SMC)

$$\mathrm{BC}_V = 5.369 - 0.7029(T_{\mathrm{eff}}/1000K)$$

. These figures show that the disagreement between theory and observed location on the H-R diagram has now disappeared, giving us some confidence in the accuracy of our new calibration.

Having both M_{bol} and T_{eff} allows us to determine the stellar radii $\mathrm{R/R}_{sun}$ from the formal definition of T_{eff}:

$$\left(\frac{R}{R_{sun}}\right) = \left(\frac{L}{L_{sun}}\right)^{\frac{1}{2}} \left(\frac{T_{eff}}{5781K}\right)^2 \tag{3.1}$$

where the numerical quantitity is the T_{eff} of the sun and $L/L_{sun} = 10^{\frac{-(M_{bol}-4.74)}{2.5}}$ (Bessell et al. 1998). The radii are listed in Table 4. The stars with the largest radii in the sample - KW Sgr, Case 75, KY Cyg, and μ Cep - all have radii of approximately 1500 R_{solar} (7 AU) for the K-band BCs (the more conservative radius measurement), making these the largest normal stars known[1]. For comparison, Betelgeuse has a radius, measured by interferometry, of 645 R_{solar} (Perrin et al. 2004). Figure B-4c includes lines of constant radii. The four stars are at the limit of predictions of current evolutionary theory, as the largest radius reached by the tracks (approximately 1500 R_{solar} is found at roughly $M_{bol} = -9$ and $\log T_{eff} = 3.57$ (3715 K).

Figures B-6 (top left and right) compare the Massey & Olsen (2003) locations of the LMC RSGs on the H-R diagram to those derived from the MARCS models. These news observations bring LMC RSGs into excellent agreement with the evolutionary tracks of Schaerer et al. (1993). The dotted lines indicate new 40 solar mass and 60 solar mass evolutionary tracks by Maeder & Meynet (2005) which show the effects of the newer opacities and an initial rotation velocity of 300 km s^{-1}.

[1]The stars VV Cep and VY CMa are thought have larger radii. VV Cep is a member of a contact binary, with the hotter companion orbiting within the atmosphere of the RSG (see discussion in Hutchings & Wright, 1971; Wright, 1977; Saito et al., 1980; Bauer & Bennett, 2000). Definition of radius by the eclipse method in this case leads to further ambiguities. VY CMa is not found to be in agreement with stellar evolutionary theory, and Humphreys et al. (2005) describe the star as "perplexing" and argue that it may be in a "unique evolutionary state".

Figures B-6 (lower left and right) compare the Massey & Olsen (2003) locations of the SMC RSGs on the H-R diagram to those derived from the MARCS models. Here the agreement with the evolutionary tracks (Charbonnel et al., 1993) is poorer, as a significant fraction of the stars appear to have effective temperatures that are still too high. There are several possible explanations for this discrepancy. The importance of rotation in massive star evolution has recently come to light (Maeder & Meynet, 2000), and one important effect is a change in the star's surface chemical composition as compared to the non-rotating case. It was initially suspected that the large scatter in the SMC was indicative of stars that began their lives with different amounts of rotation: in the metal-poor SMC, a little variation in the oxygen abundance could result in a large fractional change of molecular abudances such as TiO. However, although oxygen is a by-product of the He-burning phase, there is no expectation of oxygen enhancement at the surface during the RSG phase. The mass abundance of oxygen actually drops by about 25% as compared to the non-rotating case, and this effect is still too small to explain the dispersion of the SMC. This makes it unlikely that differences in TiO abundance can explain the increased scatter of the SMC RSGs. The full effects of rotation are not yet fully understood.

Scaling the abundances of the SMC and LMC by a single number is also not an entirely correct approximation (for a good discussion of this see Venn 1999 and Dufour 1984). The lack of individual abundances for heavy elements like oxygen would result in particularly pronounced discrepanices for these galaxies with low metal abundances where such small changes might produce observable effects in the TiO absorption lines. As improved stellar models (with improved opacities and inclusion of rotation effects) become available at the relevant mass range (10-20 solar masses) these individual abundances will be more accurately determined.

3.5 Circumstellar Dust in Red Supergiants

Initial modeling revealed a significant discrepancy between the models and the data in the NUV region (3500 Å - 4000 Å) for the reddest stars, a phenomenon first observed

in Galactic RSGs (Levesque et al., 2005) and later confirmed in the MC observations (Massey et al., 2005). This is tentatively attributed to a peculiar reddening law caused by larger-grain circumstellar dust around these stars (Massey et al. 2005). I plan to calculate this RSG-specific reddening law with additional MC data, which will be taken at the CTIO 4-meter telescope in December of 2005 (current MC data cannot be used because of the grating problem, discussed in section 2, which contaminated data at <4100 Å).

Chapter 4

Conclusions and Summary

I have determined new T_{eff} scales for red supergiants in the Milky Way and the Magellanic Clouds by fitting moderate resolution (4-6 Å) spectrophotometry with the new MARCS stellar atmosphere models. The scales are significantly warmer than previously suggested, particularly for the later M supergiants. The T_{eff} across a spectral subtype decreases by about 50 K in the LMC and 150 K in the SMC, making a Milky Way M2 I star an M1-1.5 I in the LMC and a K7-M0 in the SMC. This accounts for observed differences in average spectral type (Massey & Olsen 2003).

These newly derived physical properties bring the Galactic and LMC stars into excellent acreement with the evolutionary tracks of Maeder & Meynet (2003), but there is significantly more scatter for the SMC. This could be due to the scaling of the SMC and LMC abundances by a single number, or to the effects of rotational mixing. As improved stellar models become available this matter will be investigated further.

Further observations at the CTIO 4-meter in December are planned to derive the extinction properties of RSGs' circumstellar dust in the NUV. Extension of the temperature scale study to the metal-rich Andromeda Galaxy will allow further examinations of how metallicity affects the physical properties of these intriguing massive stars.

References

Bauer, W. H., & Bennett, P. D. 2000, PASP, 112, 31

Becker, W., & Fenkart, R. 1971, A&AS, 4, 241

Bessell, M. S., Castelli, F., & Plez, B. 1998, A&A, 333, 231

Bochkarev, N. G., & Sitnik, T. G. 1985,Ap&SS, 108, 237

Cardelli, J. A., Clayton, G. C., & Mathis, J. S. 1989, ApJ, 345, 245

Charbonnel, C., Meynet, G., Maeder, A., Schaller, G., & Schaerer, D. 1993, A&AS, 101, 415

Conti, P.S. 1976, Mem. Soc. R. Sci. Liege, 9, 193

de Zeeuw, P. T., Hoogerwerf, R., de Bruijne, J. H. J., Brown, A. G. A., & Blaauw, A. 1999, AJ, 117, 354

Dufour, R. J., 1984, in IAU Symp. 108, Structure and Evolution of the Magellani Clouds, ed. S. van den Bergh & K. S. de Boer (Dordrecht: Reidel), 353

Fernie, J. D. 1983, ApJS, 52, 7

Flower, P. J. 1975, A&A, 41, 391

Flower, P. J. 1977, A&A, 54, 31

Freytag, B., Steffen, M, & Dorch, B. 2002, Astron. Nach., 323, 213

Garmany, C. D., & Stencel, R. E. 1992, A&AS, 94, 211

Gustafsson, B., Bell, R. A., Eriksson, K., & Nordlund, Å. 1975, A&A, 42, 407

Gustafsson, B., Edvardsson, B., Eriksson, K., Mizuno-Wiedner, M., Jorgensen, U. G., & Plez, B. 2003, in ASP Conf. Ser. 288, Stellar Atmosphere Modeling, ed. I. Hubeny, D. Mihalas, & K. Werner (San Fransisco: ASP), 331

Humphreys, R. M. 1970, AJ,75, 602

Humphreys, R. M. 1978, ApJS, 38, 309

Humphreys, R. M., Davidson, K., Ruch, G., & Wallerstein, G. 2005, AJ, 129, 492

Humphreys, R. M., & McElroy, D. B. 1984, ApJ, 284, 565

Hutchings, J. B., & Wright, K. O. 1971, MNRAS, 155, 203

Barbuy & A. Renzini (Dordrecht: Kluwer), 225

Jennens, P. A. & Helfer, H. L. 1875, MNRAS, 172, 667

Johnson, H. L. 1964, Bol. Obs. Tonantzintla Tacubaya 3, 305

Johnson, H. L. 1966, ARA&A, 4, 193

Josselin, E., Blommaert, J. A. D. L., Groenewegen, M. A. T., Omont, A., & Li, F. L. 2000, A&A, 357, 225

Josselin, E., Plez, B. & Mauron, N. 2003, in IAU Symp. 210, Modelling of Stellar Atmospheres, ed. N. Piskunov, W. W. Weiss, & D. F. Gray (San Fransisco: ASP), F9

Lee, T. A. 1970, ApJ, 162, 217

Levesque, E. M., Massey, P. M., Olsen, K. A. G., Plez, B., Josselin, E., Maeder, A., & Meynet, G. 2005, ApJ, 628, 973

Levesque, E. M., Massey, P. M., Olsen, K. A. G., Plez, B., Meynet, G., & Maeder, A. 2006, ApJ, in prep

Maeder, A., & Meynet, G. 2000, ARA&A, 38, 143

Maeder et al. 1980, A&A 90L, 17

Massey, P. 1998, ApJ, 501, 153

Massey, P. 2003, ARA&A 41, 15

Massey, P. & Olsen, K. A. G. 2003, AJ 126, 2867

Massey, P., Plez, B., Levesque, E. M., Olsen, K. A. G., Clayton, G. C., & Josselin, E. 2005, ApJ, 634, 1286

Mel'Nik, A. M., & Efremov, Y. N. 1995, Pis'ma Astron. Zh., 21, 13

Mermilliod, J. C., & Paunzen, E. 2003, A&A, 404, 975

Meynet, G., & Maeder, A. 2003, A&A, 404, 975

Meynet, G., & Maeder, A. 2005, A&A, 429, 581

Moitinho, A., Emilio, J., Yun, J. L, & Phelps, R. L. 1997, AJ, 113, 1359

Morgan, W. W., & Keenan, P. C. 1973, ARA&A, 11, 29

Nicolet, B. 1978, A&AS, 34, 1

Östlin, G., & Mouhcine, M. 2005, A&A, 433, 797

Perrin, G., Ridgeway, S. T., Coude du Foresto, V., Mennesson, B., Traub, W. A., & Lacasse, M. G. 2004, A&A, 418, 675

Plez, B., 2003, in ASP Conf. Ser. 298, *GAIA* Spectroscopy: Science and Technology, ed. U. Munari (San Fransisco: ASP), 189

Plez, B., Brett, J. M., & Nordlund, Å. 1992, A&A, 256, 551

Ruprecht, J. 1966, Trans. IAU, 12B, 350

Sagar, R., & Joshi, U. C. 1981, Ap&SS, 75, 465

Saito, M., Sato, H., Saijo, K. & Hayasaka, T. 980, PASJ, 32, 163

Schaerer, D., Meynet, G., Maeder, A., & Schaller, G. 1993, A&AS, 98, 523

Schaller, G., Schaerer, D., Meynet, G., & Maeder, A. 1992, A&AS, 96, 269

Venn, K. A. 1999, ApJ, 518, 405

White, N. M., & Wing, R. F. 1978, ApJ, 222, 209

Wright, K. O. 1977, JRASC, 71, 152

Young, J. S., et al. 2000, MNRAS, 315, 635

Appendix A

Tables

Table 1. Program Stars

Star	α_{2000}	δ_{2000}	Photometry				Spectral Type		OB Association[a]	Comment
			V	$B-V$	$V-K$	Ref[b]	Old[c]	New		
BD+59 38	00 21 24.29	+59 57 11.2	9.13	2.49	···	1	M2 Iab	M2 I	Cas OB4	MZ Cas
Case 23	00 49 10.71[d]	+64 56 19.0[d]	10.72	2.77	7.80	2	M1 Iab	M3 I	Cas OB7	···
HD 236697	01 19 53.62	+58 18 30.7	8.65	2.16	5.41	3	M2 Ib	M1.5 I	NGC 457	V466 Cas
BD+59 274	01 33 29.19	+60 38 48.2	8.55	2.09	5.24	1	M0 Ib	M1 I	Cas OB8/NGC581	···
BD+60 335	01 46 05.48	+60 59 36.7	9.15	2.34	···	1	M3 Iab	M4 I	Cas OB8/NGC663	···
HD 236871	01 47 00.01	+60 22 20.3	8.74	2.27	···	2	M3 Iab	M2 I	Cas OB8	···
HD 236915	01 58 28.91	+59 16 08.7	8.30	2.20	···	2	M2 Iab	M2 I	Per OB1-A	···
BD+59 372	01 59 39.66	+60 15 01.7	9.30	2.28	···	2	K5-M0 I	K5-M0 I	Per OB1-A	···
BD+56 512	02 18 53.29	+57 25 16.7	9.23	2.47	6.99	1	M4 Ib	M3 I	Per OB1-D	BU Per
HD 14469[e]	02 22 06.89	+56 36 14.9	7.63	2.17	6.24	1	M3-4 Iab	M3-4 I	Per OB1-D	SU Per
HD 14488	02 22 24.30	+57 06 34.3	8.35	2.27	6.62	1	M4 Iab	M4 I	Per OB1-D/NGC884	RS Per
HD 14528	02 22 51.72	+58 35 11.4	9.23	2.65	7.78	1	M4e I	M4.5 I	Per OB1-D	S Per
BD+56 595	02 23 11.03	+57 11 58.3	8.18	2.23	5.42	1	M0 Iab	M1 I	Per OB1-D	···
HD 14580	02 23 24.11	+57 12 43.0	8.45	2.27	5.43	2	M0 Iab	M1 I	Per OB1-D	···
HD 14826	02 25 21.86	+57 26 14.1	8.24	2.32	6.28	2	M2 Iab	M2 I	Per OB1-D	···
HD 236979	02 38 25.42	+57 02 46.1	8.20	2.35	6.17	4	M2 Iab	M2 I	Per OB1-D?	YZ Per
W Per	02 50 37.89	+59 59 00.3	10.39	2.53	8.30	4	M3 Iab	M4.5 I	Per OB1-D?	HD 237008
BD+57 647	02 51 03.95	+57 51 19.9	9.52	2.74	···	4	M2 Iab	M2 I	Per OB1-D?	HD 237010
HD 17958	02 56 24.65	+64 19 56.8	6.24	2.03	···	1	K3 Ib	K2 I	Cam OB1	···
HD 23475[e]	03 49 31.28	+65 31 33.5	4.48	1.88	···	5	M2+ IIab	M2.5 II	···	···
HD 33299	05 10 34.98	+30 47 51.1	6.72	1.62	···	6	K1 Ib	K1 I	Aur OB1	···
HD 35601	05 27 10.22	+29 55 15.8	7.35	2.20	5.61	2	M1 Ib	M1.5 I	Aur OB1	···
HD 36389[e]	05 32 12.75	+18 35 39.2	4.38	2.07	···	1	M2 Iab-Ib	M2 I	···	···
HD 37536[f]	05 40 42.05	+31 55 14.2	6.21	2.09	5.28	3	M2 Iab	M2 I	Aur OB1	···
α Ori[e]	05 55 10.31	+07 24 25.4	0.50	1.85	···	1	M1-2 Ia-Ib	M2 I	···	···
HD 42475[e]	06 11 51.41	+21 52 05.6	6.56	2.25	5.70	3	M0-1 Iab	M1 I	Gem OB1	TV Gem
HD 42543[e]	06 12 19.10	+22 54 30.6	6.39	2.24	5.46	3	M1-2 Ia-Iab	M0 I	Gem OB1	BU Gem
HD 44537[e]	06 24 53.90	+49 17 16.4	4.91	1.97	···	1	K5-M0 Iab-Ib	M0 I	···	···
HD 50877[e]	06 54 07.95	-24 11 03.2	3.86	1.74	···	6	K2.5 Iab	K2.5 I	Coll 121	···
HD 52005[e]	07 00 15.82	+16 04 44.3	5.68	1.63	···	3	K3 Ib	K5 I	···	···
HD 52877[e]	07 01 43.15	-27 56 05.4	3.41	1.69	3.90	6	K7 Ib	M1.5 I	Coll 121	σ CMa
CD-31 4916	07 41 02.63	-31 40 59.1	8.91	2.16	5.20	1	M2 Iab	M2.5 I	NGC2439	···
HD 63302[e]	07 47 38.53	-15 59 26.5	6.35	1.78	···	5	K1 Ia-Iab	K2 I	···	···
HD 90382	10 24 25.36	-60 11 29.0	7.45	2.21	6.05	4	M3 Iab	M3-4 I	Car OB1-D	CK Car
HD 91093	10 29 35.37	-57 57 59.0	8.31	2.21	6.65	4	M2 Iab	M2 I	Car OB1-A	···
CPD-57 3502[e]	10 35 43.71	-58 14 42.3	7.44	2.02	5.17	4	M1.5 Iab-Ib	M1.5 I	Car OB1-B/NGC329	···
HD 303250	10 44 20.04	-58 03 53.5	8.92	2.51	···	4	M3 Iab	M2 I	Car OB1-B?	···

Table 1—Continued

Star	α_{2000}	δ_{2000}	Photometry				Spectral Type		OB Association[a]	Comment
			V	$B-V$	$V-K$	Ref[b]	Old[c]	New		
CD-58 3538[e]	10 44 47.15	-59 24 48.1	8.36	2.31	6.54	4	M2+ Ia-0	M2 I	Car OB1-E	RT Car
HD 93420[e]	10 45 50.63	-59 29 19.5	7.55	1.87	6.15	4	M4 Ib	M4 I	Car OB1-E	BO Car
HD 94096	10 50 26.30	-59 58 56.5	7.38	2.24	5.64	4	M2 Iab	M2 I	Car OB1-E	IX Car
HD 95687	11 01 35.76	-61 02 55.8	7.35	2.12	5.81	4	M2 Iab	M3 I	Car OB2	···
HD 95950	11 03 06.15	-60 54 38.6	6.75	2.04	5.18	4	M2 Ib	M2 I	Car OB2	···
HD 97671	11 13 29.97	-60 05 28.8	8.39	2.52	7.42	4	M3 Ia	M3-4 I	Car OB2[g]	···
CD-60 3621	11 35 44.96	-61 34 41.0	7.27	1.92	4.74	4	M0 Ib	M1.5 I	NGC3766	···
HD 100930[e]	11 36 26.22	-61 19 10.0	7.78	1.95	5.68	4	M2.5 Iab-Ib	M2.5 I	···	···
CD-60 3636	11 36 34.84	-61 36 35.1	7.62	1.81	···	4	M0 Ib	M0 I	NGC3766	···
V396 Cen	13 17 25.05	-61 35 02.3	7.85	2.15	6.74	4	M4 Ia-Iab	M3-4 I	Cen OB1-D	HD 115283
CPD-53 7344	16 12 56.91	-54 13 13.8	8.79	1.78	···	4	K2 Ib	K2 I	NGC6067	···
CPD-53 7364	16 13 04.01[d]	-54 12 21.2[d]	9.13	1.86	···	4	K4 Ib	K2 I	NGC6067	···
HD 160371[e]	17 40 58.55	-32 12 52.1	6.14	1.82	···	1	K2.5 Ib	K2.5 I	M6	BM Sco
α Her[c]	17 14 38.86	+14 23 25.2	3.06	1.45	···	3	M5 Ib-II	M5 I	···	···
KW Sgr	17 52 00.73	-28 01 20.5	9.35	2.78	7.98	4	M3 Ia	M1.5 I	Sgr OB5	HD 316496
HD 175588[e]	18 54 30.28	+36 53 55.0	4.30	1.67	···	5	M4 II	M4 II	···	δ^2 Lyr
HD 181475[e]	19 20 48.31	-04 30 09.0	6.96	2.14	···	6	M0 II	M1 II	···	···
HD 339034	19 50 11.93	+24 55 24.2	9.36	3.05	···	1	M1 Ia	K3 I	Vul OB1	Case 15
BD+35 4077	20 21 12.37	+35 37 09.8	9.72	2.93	8.11	3	M3 Iab	M2.5 I	Cyg OB1	···
BD+36 4025	20 21 21.88	+36 55 55.7	9.33	2.49	8.75	3	M3 Ia	M3-4 I	Cyg OB1	BI Cyg
BD+37 3903	20 21 38.55	+37 31 58.9	9.97	3.26	9.75	3	M3.5 Ia	M3 I	Cyg OB1	BC Cyg
KY Cyg	20 25 58.08[d]	+38 21 07.0[d]	10.57	3.64	10.40	4	M3 Ia	M3-4 I	Cyg OB1	Case 66
BD+39 4208[e]	20 28 50.59	+39 58 54.4	8.69	2.87	8.21	1	M3-4 Ia-Iab	M3 I	Cyg OB9	RW Cyg
HD 200905[e]	21 04 55.86	+43 55 40.2	3.70	1.65	···	5	K4.5 Ib-II	K4.5 I	···	···
HD 202380[e]	21 12 47.25	+60 05 52.8	6.62	2.39	···	2	M2- Ib	M2 I	Cep OB2-A	···
HR 8248	21 33 17.89	+45 51 14.4	6.23	1.78	···	7	K4 Ib	K1 I	Cyg OB7	HD 205349
HD 206936[e]	21 43 30.46	+58 46 48.1	4.08	2.35	5.96	1	M2 Ia	M1 I	Cep OB2-A	μ Cep
HD 210745[e]	22 10 51.28	+58 12 04.5	3.35	1.55	···	5	K1.5 Ib	K1.5 I	···	···
BD+56 2793	22 30 10.73	+57 00 03.1	8.09	2.28	6.22	3	M2 Ia	M3 I	Cep OB2-B	HD 239978, ST Cep
Case 75	22 33 35.0	+58 53 45	10.67	3.18	···	4	M1 Ia	M2.5 I	Cep OB1[g]	V354 Cep[h]
Case 78	22 49 10.8	+59 18 11	10.76	2.30	···	4	M2 Ib	M2 I	Cep OB1[g]	V355 Cep[h]
HD 216946[e]	22 56 26.00	+49 44 00.8	4.94	1.77	···	5	M0- Ib	M0 I	Lac OB1[h]	···
Case 80	23 10 10.90	+61 14 29.9	9.72	2.60	···	4	M2 Iab	M3 I	Cas OB2	GU Cep
Case 81	23 13 31.50[d]	+60 30 18.5[d]	9.92	2.70	···	4	M2 Ia	M2 I	Cas OB2	V356 Cep?
HD 219978	23 19 23.77	+62 44 23.2	6.77	2.27	···	2	K5 Ib	M1 I	Cep OB3	V809 Cas
BD+60 2613	23 44 03.28	+61 47 22.2	8.50	2.77	7.48	1	M4 Ia	M3 I	Cas OB5	PZ Cas
BD+60 2634	23 52 56.24	+61 00 08.3	9.17	2.51	7.22	3	M2 Iab	M3 I	Cas OB5	TZ Cas

Table 1—Continued

Star	α_{2000}	δ_{2000}	Photometry				Spectral Type		OB Association[a]	Comment
			V	$B-V$	$V-K$	Ref[b]	Old[c]	New		
SMC005092	00 45 04.56	-73 05 27.4	12.90	2.03	4.83	8	M1 I	M2 I	···	···
SMC008930	00 47 36.94	-73 04 44.3	12.68	2.00	4.36	8	K7 I	M0 I	···	···
SMC010889	00 48 27.02	-73 12 12.3	12.20	2.00	4.43	8	K7 I	M0 I	···	···
SMC011101	00 48 31.92	-73 07 44.4	13.54	1.69	4.30	8	K7 I	K2.5 I	···	···
SMC011709	00 48 46.32	-73 28 20.7	12.43	1.79	3.90	8	K7 I	K5-M0 I	···	···
SMC011939	00 48 51.83	-73 22 39.3	12.82	1.81	4.21	8	M0 I	K2 I	···	···
SMC012322	00 49 00.32	-72 59 35.7	12.44	1.93	4.16	8	M0 I	K5-M0 I	···	···
SMC013740	00 49 30.34	-73 26 49.9	13.47	1.77	4.08	8	K7 I	K3 I	···	···
SMC013951	00 49 34.42	-73 14 09.9	13.00	1.79	3.94	8	K7 I	K3 I	···	···
SMC015510	00 50 06.42	-73 28 11.1	12.59	1.90	4.06	8	M0 I	K5 I	···	···
SMC018136	00 50 56.01	-72 15 05.7	11.98	1.95	4.13	8	M0 I	M0 I	···	···
SMC020133	00 51 29.68	-73 10 44.3	12.33	1.95	4.18	8	M0 I	M0 I	···	···
SMC021362	00 51 50.25	-72 05 57.2	12.89	1.86	4.07	8	K5-M0 I	K5 I	···	···
SMC021381	00 51 50.46	-72 11 32.2	12.81	1.81	3.81	8	K5-M0 I	K5 I	···	···
SMC023401	00 52 25.36	-72 25 13.3	12.99	1.71	3.56	8	K5 I	K1 I	···	···
SMC023743	00 52 31.49	-72 11 37.3	12.98	1.65	3.57	8	K5-M0 I	K2 I	···	···
SMC025879	00 53 08.87	-72 29 38.6	11.91	1.77	3.46	8	K7 I	M0 I	···	···
SMC030135	00 54 26.90	-72 52 59.4	12.84	1.68	3.35	8	K0-2 I	K2 I	···	···
SMC030616	00 54 35.90	-72 34 14.3	12.22	1.85	3.88	8	K7 I	K2 I	···	···
SMC034158	00 55 36.58	-72 36 23.6	12.79	1.78	3.88	8	K7 I	K2 I	···	···
SMC035445	00 55 58.84	-73 20 41.4	12.74	1.77	3.76	8	M0 I	K1 I	···	···
SMC042438	00 58 08.71	-72 19 26.7	13.20	1.59	3.84	8	K3-5 I	K2 I	···	···
SMC043219	00 58 23.30	-72 48 40.7	13.06	1.84	3.95	8	M0 I	K2 I	···	···
SMC045378	00 59 07.16	-72 13 08.6	12.93	1.56	3.93	8	K5 I	K3 I	···	···
SMC046497	00 59 31.33	-72 15 46.4	12.40	1.98	4.09	8	M1 I	K5-M0 I	···	···
SMC046662	00 59 35.04	-72 04 06.2	12.90	1.88	4.55	8	M2 I	K3 I	···	···
SMC048122	01 00 09.42	-72 08 44.5	12.19	1.78	3.46	8	K3 I	K1 I	···	···
SMC049478	01 00 41.56	-72 10 37.0	12.17	1.81	4.21	8	M0 I	K5-M0 I	···	···
SMC050028	01 00 55.12	-71 37 52.6	11.81	1.82	3.77	8	M0 I	K1 I	···	···
SMC050840	01 01 15.99	-72 13 10.0	12.57	1.95	4.20	8	M1-2 I	M1 I	···	···
SMC054708	01 02 51.37	-72 24 15.5	12.82	1.81	3.74	8	K0 I	K1 I	···	···
SMC055681	01 03 12.98	-72 09 26.5	12.52	1.65	3.93	8	M3 I	K5-M0 I	···	···
SMC056732	01 03 34.30	-72 06 05.8	12.86	1.53	4.00	8	K7 I	K5-M0 I	···	···
SMC057386	01 03 47.35	-72 01 16.0	12.71	1.57	3.74	8	K3-5 I	K1 I	···	···
SMC057472	01 03 48.89	-72 02 12.7	12.80	1.83	3.83	8	K5-7 I	K2 I	···	···
SMC059803	01 04 38.16	-72 01 27.2	11.98	1.95	3.88	8	M0-1 I	K2-3 I	···	···
SMC060447	01 04 53.05	-72 47 48.5	13.09	1.64	3.91	8	M0 I	K2 I	···	···

Table 1—Continued

Star	α_{2000}	δ_{2000}	Photometry				Spectral Type		OB Association[a]	Comment
			V	$B-V$	$V-K$	Ref[b]	Old[c]	New		
SMC067509	01 08 13.34	-72 00 02.9	12.74	1.68	3.57	8	K2 I	K1 I	...	...
SMC069886	01 09 38.08	-73 20 01.9	11.74	1.95	3.95	8	M2 I	K5-M0 I	...	...
LMC054365	05 02 09.57	-70 25 02.4	13.26	1.85	4.94	8	M3 I	M2.5 I	...	...
LMC061753	05 03 59.77	-69 38 15.0	13.16	2.07	5.14	8	M2 I	M2 I	...	...
LMC062090	05 04 05.10	-70 22 46.7	12.50	1.96	4.39	8	M1 I	M1 I	...	...
LMC064048	05 04 41.79	-70 42 37.2	13.28	1.89	5.25	8	M3 I	M2.5 I	...	...
LMC065558	05 05 10.03	-70 40 03.2	12.62	1.89	4.24	8	M0 I	M1 I	...	...
LMC067982	05 05 56.61	-70 35 24.0	12.76	1.93	4.65	8	M4.5 I	M2.5 I	...	...
LMC068098	05 05 58.92	-70 29 14.6	13.11	1.90	4.64	8	M1 I	M1.5 I	...	...
LMC068125	05 05 59.56	-70 48 11.4	13.43	1.83	5.12	8	M4 I	M4 I	...	...
LMC109106	05 17 56.51	-69 40 25.4	12.96	1.85	4.39	8	M2 I	M2.5 I	...	...
LMC116895	05 19 53.34	-69 27 33.4	12.43	1.92	4.21	8	M3 I	M0 I	...	...
LMC119219	05 20 23.69	-69 33 27.3	12.14	2.04	4.16	8	M3 I	M3 I	...	...
LMC131735	05 23 34.09	-69 19 07.0	12.65	1.84	3.75	8	K7 I	K2 I	...	...
LMC134383	05 25 44.95	-69 04 48.9	13.46	1.65	5.47	8	M3 I	M2.5 I	...	...
LMC135720	05 26 27.52	-69 10 55.5	13.57	1.85	5.86	8	M3 I	M4.5 I	...	...
LMC136042	05 26 34.92	-68 51 40.1	12.24	1.08	4.97	8	M1 I	M3 I	...	...
LMC137624	05 27 10.38	-69 16 17.6	13.16	1.88	4.38	8	M0 I	M0 I	...	...
LMC137818	05 27 14.33	-69 11 10.7	13.33	1.74	5.14	8	M3 I	M2 I	...	...
LMC138405	05 27 26.86	-69 00 02.0	13.08	1.83	4.41	8	M0 I	M1 I	...	...
LMC140296	05 28 06.11	-69 07 13.5	13.12	1.87	4.97	8	M1-2 I	M2 I	...	...
LMC141430	05 28 28.98	-68 07 07.8	12.30	2.15	4.82	8	M0[i]I	M1 I	...	...
LMC142202	05 28 45.59	-68 58 02.3	12.15	1.65	4.60	8	M0-M1 I	M1.5 I	...	...
LMC142907	05 29 00.86	-68 46 33.6	13.05	1.89	4.61	8	M1 I	M2 I	...	...
LMC143877	05 29 21.10	-68 47 31.5	11.82	1.94	3.85	8	K7 I	K3 I	...	...
LMC146126	05 30 02.36	-67 02 45.0	11.17	1.80	3.20	8	K5 I	K5 I	...	...
LMC147199	05 30 21.00	-67 20 05.7	12.73	1.57	5.28	8	M4 I	M1.5 I	...	...
LMC149721	05 31 03.50	-69 05 40.0	12.71	1.86	4.13	8	K5-7 I	M0 I	...	...
LMC157533	05 33 29.67	-67 31 38.0	13.16	1.50	4.34	8	K5 I	K5 I	...	...
LMC158317	05 33 44.60	-67 24 16.9	13.35	1.96	4.86	8	M 2 I	M1 I	...	...
LMC159974	05 34 21.49	-69 21 59.8	12.72	1.77	3.83	8	K2-5 I	K1 I	...	...
LMC169754	05 37 58.77	-69 14 23.7	13.21	2.15	4.83	8	K2-3 I	K2 I	...	...
LMC174714	05 40 24.48	-69 21 16.6	13.13	1.98	5.28	8	M4-5 I	M1.5 I	...	...
LMC175464	05 40 55.36	-69 23 25.0	12.90	2.20	5.36	8	M2-3 I	M2 I	...	...
LMC175746	05 41 06.94	-69 17 14.8	13.30	2.06	5.53	8	M3 I	M3 I	...	...
LMC176890	05 41 50.26	-69 21 15.7	12.85	1.97	4.29	8	K7 I	M0 I	...	...
LMC177150	05 42 00.84	-69 11 37.0	13.80	1.89	5.12	8	M1 I	M1.5 I	...	...

Table 1—Continued

Star	α_{2000}	δ_{2000}	Photometry				Spectral Type		OB Association[a]	Comment
			V	$B-V$	$V-K$	Ref[b]	Old[c]	New		
LMC177997	05 42 35.48	-69 08 48.3	12.56	2.02	4.85	8	M2[i] I	M1.5 I	...	...

[a]OB association membership from Humphreys (1978) and Garmany & Stencel (1992). For Per OB1 and Car OB1, the sub-groups identified by Mel'Nik & Efremov (1995) have been used, based upon the star's l and b.

[b] References for V and $B-V$: (1) Nicolet (1978); (2) Humphreys (1970); (3) Lee (1970); (4) Humphreys (1978) and references therein; (5) Johnson et al. (1966); (6) Fernie (1983); (7) Jennens & Helfer (1975); (8) Massey (2002). The K data come from Josselin et al. (2000) and references therein for the Galactic sources, and the 2Mass (K_s) point-source catalog for the MC sources.

[c]Old spectral types for Galactic sources are from Humphreys (1978) and references therein, except for the standard stars, for which the types are from Morgan & Keenen (1973). Old spectral types for the MC sources are from Massey & Olsen (2003).

[d]Coordinates new to this study, listed incorrectly in Humphreys et al. (1970) and Humphreys (1978) respectively.

[e]Spectral standard from Morgan & Keenan (1973).

[f]Possible AGB; see Josselin et al. (2003).

[g]Membership listed as questionable by Humphreys (1978), but see also Garmany & Stencel (1992).

[h]Incorrectly cross-referenced to the BD catalog by Garmany & Stencel (1992).

[i]Old spectral type from Elias et al. (1985).

Table 2. Adopted Distance Moduli and Average Reddenings

OB Assoc./Cluster[a]	l	b	$(m-M)_o$ [mag]					$E(B-V)_{\rm cluster}$	Additional
			Value	Ref.[b]	Value	Ref.[b]	Adopted	[mag]	$(m-M)_o$, (Ref.[b])
Cas OB4	119.5	-0.4	11.0	1	12.3	2	11.6	0.70 ± 0.21	···
Cas OB7	123.5	0.9	12.0	2	···	···	12.0	0.83 ± 0.14	···
NGC 457	126.6	-4.4	12.0	2	11.9	3	11.9	0.51 ±	···
Cas OB8/NGC581	128.0	-1.8	11.9	4	11.7	3	11.8	0.38	···
Cas OB8/NGC663	129.5	-1.0	11.6	4	11.5	3	11.5	0.78	···
Cas OB8	129.4	-0.9	11.2	1	12.3	2	11.7	0.69 ± 0.19	···
Per OB1-A	131.1	-1.5	11.0	1	11.8	2	11.4	0.66 ± 0.19	···
Per OB1-D	135.0	-3.5	11.4	1	11.8	2	11.4	0.66± 0.19	···
Per OB1-D/NGC 884	135.1	-3.6	12.0	4	11.9	3	11.9	0.56	···
Cam OB1	140.4	1.9	10.0	1	10.0	2	10.0	0.74 ± 0.21	···
Aur OB1	174.6	1.2	10.7	1	10.6	2	10.7	0.47 ± 0.15	···
Gem OB1	188.9	3.4	10.6	1	10.9	2	10.7	0.66 ± 0.24	···
Coll 121	237.9	-7.7	8.9	5	8.4	3	8.4	0.03	···
NGC 2439	246.4	-4.4	13.2	2	12.9	3	13.0	0.57 ± 0.24	···
Car OB1-A	284.5	-0.0	11.9	1	12.0	2	11.9	0.48 ± 0.11	···
Car OB1-B/NGC 3293	285.9	+0.1	12.0	2	11.8	3	11.9	0.30	···
Car OB1-B	286.0	0.5	11.7	1	12.0	2	11.9	0.55 ± 0.21	···
Car OB1-D	286.6	-1.8	11.9	1	12.0	2	11.7	0.55 ± 0.21	···
Car OB1-E	287.6	-0.7	12.1	1	12.0	2	12.0	0.55 ± 0.21	···
Car OB2	290.6	-0.1	11.7	1	11.5	2	11.6	0.48 ± 0.18	···
NGC 3766	294.1	-0.0	11.6	1	11.7	6	11.6	0.20 ± 0.10	11.2 (3)
Cen OB1-D	305.5	1.6	11.4	1	12.0	2	11.6	0.75 ± 0.25	···
NGC 6067	329.8	-2.2	11.6	2	10.8	3	10.8	0.32 ± 0.07	···
M 6	356.6	-0.7	8.3:	2	8.4	3	8.4	0.14	···
Sgr OB5	0.2	-1.3	12.4	2	···	···	12.4	0.92 ± 0.33	···
Vul OB1	59.4	-0.1	12.0	1	11.5	2	11.8	0.94 ± 0.20	12.7 (7)
Cyg OB1	75.6	1.1	10.7	1	11.3	2	11.0	0.93 ± 0.33	···
Cyg OB9	76.8	1.4	10.7	1	10.4	2	10.6	1.22 ± 0.32	···
Cep OB2-A	99.3	3.8	9.9	1	9.6	2	9.7	0.66 ± 0.19	9.0 (5)
Cep OB2-B	103.6	5.6	9.4	1	9.6	2	9.5	0.66 ± 0.19	9.0 (5)
Cep OB1	108.5	-2.7	11.7	1	12.7	2	12.2	0.63 ± 0.17	···
Cyg OB7	90.0	2.0	9.5	2	9.6	8	9.5	0.65 ± 0.40:	···
Lac OB1	96.8	16.1	9.0	1	8.9	9	8.9	0.11:	7.8 (5)
Cas OB2	112.0	0.0	12.1	2	···	···	12.1	0.99 ± 0.25	
Cep OB3	110.4	2.9	9.6	1	9.7	2	9.7	0.84 ± 0.10	···
Cas OB5	115.5	0.3	11.8	1	12.0	2	11.9	0.60 ± 0.14	···

[a]Either classical names, or in the case of the sub-divided associations, taken from Mel'Nik & Efremov 1995.

[b]References: (1) Mel'Nik & Efremov 1995; (2) Humphreys 1978; (3) WEBDA (Mermilliod & Paunzen 2003); (4) Becker & Fenkart 1971; (5) de Zeeuw et al 1999; (6) Moitinho et al. 1997; (7) Sagar & Joshi 1981; (8) Bochkarev & Sitnik 1985; (9) Ruprecht 1966.

Table 3. Observation Parameters

	KPNO 2.1-m		CTIO 1.5-m			CTIO 4-m	
	BLUE	RED	BLUE	ORANGE	RED	BLUE	RED
Grating/l mm^{-1}	26/600	58/400	26/600	58/400	58/400	KPGL1/632	KPGLF/632
Blocking Filter	none	GG495	none	GG495	OG570	GG345	GG495
Wavelength Coverage(Å)	3200 - 6000	5000 - 9000	3500 -5200	5000 - 7500	6300 - 9000	3550 - 6420	6130 - 9100
Slit Width (μm)	170	250	270	200	200	375	375
Resolution(Å)	3.6	5.7	5.0	6.4	6.4	3.8	3.8

Table 4. Results of Model Fits

Star	Spectral Type	$T_{\rm eff}$	A_V	log g		R/R_o[a,b]	M_V[b]	$M_{\rm bol}$[a,b]
				Model	Actual[c]			
BD+59 38	M2 I	3650	3.10	0.0	0.1	600	-5.57	-7.17
Case 23	M3 I	3600	3.25	0.5	0.3	410	-4.53	-6.28
HD 236697	M1.5 I	3700	1.55	0.5	0.4	380	-4.80	-6.25
BD+59 274	M1 I	3750	1.55	0.5	0.4	360	-4.80	-6.14
BD+60 335	M4 I	3525	2.63	0.0	0.1	610	-4.99	-7.05
HD 236871	M2 I	3625	2.17	0.0	0.2	520	-5.13	-6.80
HD 236915	M2 I	3650	1.71	0.0	0.3	420	-4.80	-6.40
BD+59 372	K5-M0 I	3825	2.48	0.5	0.6	290	-4.58	-5.77
BD+56 512	M3 I	3600	3.25	0.5	0.1	620	-5.42	-7.17
HD 14469	M3-4 I	3575	2.01	0.0	-0.1	780	-5.78	-7.64
HD 14488	M4 I	3550	2.63	0.0	-0.3	1000	-6.18	-8.15
HD 14528	M4.5 I	3500	4.18	-0.5	-0.4/-0.1	1230/780	-6.36	-8.53/-7.53
BD+56 595	M1 I	3800	1.86	0.0	0.4	380	-5.08	-6.31
HD 14580	M1 I	3800	2.17	0.5	0.4	380	-5.12	-6.35
HD 14826	M2 I	3625	2.48	0.0	0.0	650	-5.64	-7.31
HD 236979	M2 I	3700	2.32	0.0	0.2	540	-5.52	-6.97
W Per	M4.5 I	3550	4.03	0.0	0.1	620	-5.13	-7.09
BD+57 647	M2 I	3650	4.03	0.0	0.0	710	-5.91	-7.51
HD 17958	K2 I	4200	2.17	0.5	0.5	360	-5.93	-6.63
HD 23475	M2.5 II	3625	1.08	0.0	...	...	...	...
HD 33299	K1 I	4300	0.77	0.5	0.9	190	-4.76	-5.37
HD 35601	M1.5 I	3700	2.01	0.0	0.2	500	-5.36	-6.81
HD 36389	M2 I	3650	1.24	0.0	...	...	...	...
HD 37536	M2 I	3700	1.39	0.0	0.1	630	-5.88	-7.33
α Ori	M2 I	3650	0.62	0.0	...	...	...	...
HD 42475	M1 I	3700	2.17	0.0	-0.1	770	-6.31	-7.76
HD 42543	M0 I	3800	2.01	0.0	0.0	670	-6.32	-7.55
HD 44537	M0 I	3750	0.62	0.0	...	...	...	...
HD 50877	K2.5 I	3900	0.16	0.5	0.6	280	-4.69	-5.75
HD 52005	K5 I	3900	0.00	0.0	...	...	...	...
HD 52877	M1.5 I	3750	0.16	0.5	0.3	420	-5.14	-6.48
CD-31 4916	M2.5 I	3600	2.01	0.0	-0.1/0.2	850/500	-6.11	-7.85/-6.69
HD 63302	K2 I	4100	0.62	0.0	...	...	...	...
HD 90382	M3-4 I	3550	1.86	0.0	-0.3	1060	-6.31	-8.27
HD 91093	M2 I	3625	2.01	0.0	0.0	640	-5.60	-7.28
CPD-57 3502	M1.5 I	3700	1.08	0.0	0.2	540	-5.54	-6.99
HD 303250	M2 I	3625	2.94	0.0	-0.1	750	-5.92	-7.60

Table 4—Continued

Star	Spectral Type	$T_{\rm eff}$	A_V	$\log g$		R/R_o[a,b]	M_V[b]	$M_{\rm bol}$[a,b]
				Model	Actual[c]			
CD-58 3538	M2 I	3625	3.10	0.0	-0.3	1090	-6.74	-8.41
HD 93420	M4 I	3525	1.08	0.0	-0.1	790	-5.53	-7.60
HD 94096	M2 I	3650	1.86	0.0	-0.2	920	-6.48	-8.08
HD 95687	M3 I	3625	1.71	0.0	-0.1	760	-5.96	-7.63
HD 95950	M2 I	3700	1.24	0.0	0.0	700	-6.09	-7.54
HD 97671	M3-4 I	3550	2.63	0.0	-0.2	860	-5.85	-7.81
CD-60 3621	M1.5 I	3700	0.77	0.0	0.3	440	-5.11	-6.55
HD 100930	M2.5 I	3600	1.08	0.0	...	...	...	...
CD-60 3636	M0 I	3800	0.77	0.5	0.5	320	-4.76	-5.98
V396 Cen	M3-4 I	3550	2.48	0.0	-0.3	1070	-6.33	-8.29
CPD-53 7344	K2 I	4000	0.77	1.0	1.3	100	-2.78	-3.70
CPD-53 7364	K2 I	4000	1.08	1.0	1.3	100	-2.76	-3.67
HD 160371	K2.5 I	3900	0.31	1.0	1.3	100	-2.57	-3.63
α Her[d]	M5 I	3450	1.40	0.0	...	...	...	...
KW Sgr	M1.5 I	3700	4.65	-0.5	-0.5	1460	-7.70	-9.15
HD 175588	M4 II	3550	0.47	0.0	...	...	...	...
HD 181475	M1 II	3700	1.39	0.0	...	...	...	...
HD 339034	K3 I	4000	5.27	0.0	-0.2	980	-7.71	-8.63
BD+35 4077	M2.5 I	3600	5.27	0.0	-0.3/0.1	1040/620	-6.55	-8.30/-7.18
BD+36 4025	M3-4 I	3575	5.11	-0.5	-0.4	1240	-6.78	-8.64
BD+37 3903	M3 I	3575	5.58	-0.5	-0.3	1140	-6.61	-8.46
KY Cyg	M3-4 I	3500	7.75	-1.0	-0.9/-0.5	2850/1420	-8.18	-10.36/-8.84
BD+39 4208	M3 I	3600	4.49	0.0	-0.2	980	-6.41	-8.15
HD 200905	K4.5 I	3800	0.00[e]	0.0[ee]	...	...	...	...
HD 202380	M2 I	3700	2.63	0.0	0.1	590	-5.72	-7.16
HR 8248	K1 I	4000	0.93	1.0	0.9	200	-4.20	-5.12
HD 206936	M1 I	3700	2.01	-0.5	-0.5	1420	-7.63	-9.08
HD 210745	K1.5 I	4000	0.00	0.0	...	...	...	...
BD+56 2793	M3 I	3600	2.32	0.5	0.6	290	-3.73	-5.48
Case 75	M2.5 I	3650	6.05	-0.5	-0.5	1520	-7.57	-9.17
Case 78	M2 I	3650	4.65	0.0	-0.1	770	-6.09	-7.69
HD 216946	M0 I	3800	0.31	0.5	0.7	260	-4.27	-5.50
Case 80	M3 I	3625	2.94	0.0	0.1	570	-5.32	-7.00
Case 81	M2 I	3700	3.56	0.0	0.1	590	-5.74	-7.19
HD 219978	M1 I	3750	2.17	0.5	0.4	410	-5.10	-6.44
BD+60 2613	M3 I	3600	4.49	-0.5	-0.7/-0.4	1940/1190	-7.89	-9.64/8.57
BD+60 2634	M3 I	3600	3.25	0.0	-0.1	800	-5.98	-7.73

Table 4—Continued

Star	Spectral Type	$T_{\rm eff}$	A_V	$\log g$		R/R_o[a,b]	M_V[b]	$M_{\rm bol}$[a,b]
				Model	Actual[c]			
SMC005092	M2 I	3475	0.40	-0.5	-0.4	1220	-6.40	-8.48
SMC008930	M0 I	3625	0.56	0.0	-0.3	1070	-6.78	-8.38
SMC010889	M0 I	3600	0.09	-0.5	-0.3	1130	-6.79	-8.47
SMC011101	K2.5 I	4200	1.43	0.0	0.2	540	-6.79	-7.55
SMC011709	K5-M0 I	3725	0.09	0.0	-0.1	830	-6.56	-7.93
SMC011939	K2 I	4025	1.05	0.0	0.0	750	-7.13	-8.05
SMC012322	K5-M0 I	3750	0.56	0.0	-0.2	980	-7.02	-8.34
SMC013740	K3 I	3750	0.34	0.0	0.2	550	-5.77	-7.09
SMC013951	K3 I	4225	1.12	0.0	0.2	590	-7.02	-7.76
SMC015510	K5 I	3850	0.68	0.0	-0.1	850	-6.99	-8.13
SMC018136	M0 I	3575	0.09	-0.5	-0.4	1310	-7.01	-8.76
SMC020133	M0 I	3625	0.22	-0.5	-0.3	1080	-6.79	-8.39
SMC021362	K5 I	3775	0.25	0.0	0.0	670	-6.26	-7.53
SMC021381	K5 I	3800	0.28	0.0	0.0	680	-6.37	-7.59
SMC023401	K1 I	4075	0.40	0.0	0.3	490	-6.31	-7.18
SMC023743	K2 I	4050	0.25	0.0	0.3	470	-6.17	-7.06
SMC025879	M0 I	3700	0.03	-0.5	-0.3	1060	-7.02	-8.44
SMC030135	K2 I	4050	0.28	0.0	0.2	510	-6.34	-7.23
SMC030616	K2 I	3850	0.40	0.0	-0.1	880	-7.08	-8.22
SMC034158	K2 I	4075	0.90	0.0	0.1	670	-7.01	-7.88
SMC035445	K1 I	4100	0.65	0.0	0.1	600	-6.81	-7.66
SMC042438	K2 I	4250	0.99	0.0	0.3	500	-6.69	-7.41
SMC043219	K2 I	3850	0.28	0.0	0.2	570	-6.12	-7.26
SMC045378	K3 I	3850	0.47	0.0	0.1	660	-6.43	-7.58
SMC046497	K5-M0 I	3700	0.37	0.0	-0.2	990	-6.87	-8.30
SMC046662	K3 I	4100	1.24	0.0	0.0	730	-7.24	-8.08
SMC048122	K1 I	4225	0.81	0.0	0.0	740	-7.52	-8.26
SMC049478	K5-M0 I	3700	0.34	0.0	-0.3	1080	-7.07	-8.49
SMC050028	K1 I	4300	1.36	0.0	-0.2	1080	-8.45	-9.14
SMC050840	M1 I	3625	0.19	0.0	-0.2	950	-6.52	-8.12
SMC054708	K1 I	4300	0.99	0.0	0.2	570	-7.07	-7.76
SMC055681	K5-M0 I	4100	1.18	0.0	-0.1	850	-7.56	-8.40
SMC056732	K5-M0 I	3725	0.25	0.0	0.0	730	-6.29	-7.66
SMC057386	K1 I	4300	0.87	0.0	0.2	570	-7.06	-7.74
SMC057472	K2 I	4100	0.65	0.0	0.2	580	-6.75	-7.60
SMC059803	K2-3 I	4100	0.93	0.0	-0.2	970	-7.85	-8.69
SMC060447	K2 I	3900	0.50	0.0	0.1	580	-6.31	-7.37

Table 4—Continued

Star	Spectral Type	$T_{\rm eff}$	A_V	$\log g$		R/R_o[a,b]	M_V[b]	$M_{\rm bol}$[a,b]
				Model	Actual[c]			
SMC067509	K1 I	4175	0.56	0.0	0.2	540	-6.72	-7.50
SMC069886	K5-M0 I	3750	0.28	-0.5	-0.3	1190	-7.44	-8.76
LMC054365	M2.5 I	3525	0.56	0.0	-0.2	900	-5.80	-7.88
LMC061753	M2 I	3600	0.68	0.0	-0.1	830	-6.02	-7.80
LMC062090	M1 I	3700	0.47	0.0	-0.1	830	-6.47	-7.92
LMC064048	M2.5 I	3500	0.40	0.0	-0.2	880	-5.62	-7.81
LMC065558	M1 I	3725	0.31	0.0	0.0	700	-6.19	-7.57
LMC067982	M2.5 I	3575	0.65	0.0	-0.3	1040	-6.39	-8.27
LMC068098	M1.5 I	3700	0.56	0.0	0.0	650	-5.95	-7.40
LMC068125	M4 I	3475	0.84	0.0	-0.3	1080	-5.91	-8.21
LMC109106	M2.5 I	3550	0.37	0.0	-0.2	890	-5.91	-7.89
LMC116895	M0 I	3750	0.71	0.0	-0.2	880	-6.78	-8.10
LMC119219	M3 I	3575	0.25	-0.5	-0.3	1150	-6.61	-8.48
LMC131735	K2 I	4150	0.77	0.0	0.2	510	-6.62	-7.36
LMC134383	M2.5 I	3575	0.77	0.0	-0.1	800	-5.81	-7.69
LMC135720	M4.5 I	3425	0.90	-0.5	-0.4	1200	-5.83	-8.38
LMC136042	M3 I	3500	0.09	-0.5	-0.4	1240	-6.35	-8.54
LMC137624	M0 I	3700	0.40	0.0	0.1	600	-5.74	-7.19
LMC137818	M2 I	3625	0.71	0.0	-0.1	740	-5.88	-7.57
LMC138405	M1 I	3675	0.40	0.0	0.0	650	-5.82	-7.35
LMC140296	M2 I	3625	1.15	0.0	-0.2	990	-6.53	-8.22
LMC141430	M1 I	3700	0.90	-0.5	-0.3	1110	-7.10	-8.55
LMC142202	M1.5 I	3650	0.40	-0.5	-0.3	1050	-6.75	-8.36
LMC142907	M2 I	3650	0.68	0.0	-0.1	790	-6.13	-7.74
LMC143877	K3 I	3900	0.90	0.0	-0.2	1010	-7.58	-8.58
LMC146126	K5 I	3875	0.25	0.0	-0.2	1050	-7.58	-8.62
LMC147199	M1.5 I	3675	0.53	0.0	-0.1	810	-6.30	-7.82
LMC149721	M0 I	3750	0.40	0.0	0.0	670	-6.19	-7.51
LMC157533	K5 I	3825	0.53	0.0	0.2	510	-5.87	-7.00
LMC158317	M1 I	3675	0.77	0.0	0.0	680	-5.92	-7.45
LMC159974	K1 I	4300	1.24	0.0	0.2	560	-7.02	-7.72
LMC169754	K2 I	4100	1.95	0.0	0.0	700	-7.24	-8.01
LMC174714	M1.5 I	3625	1.33	0.0	-0.3	1080	-6.70	-8.39
LMC175464	M2 I	3625	1.33	-0.5	-0.4	1200	-6.93	-8.62
LMC175746	M3 I	3550	1.18	0.0	-0.3	1100	-6.38	-8.35
LMC176890	M0 I	3750	0.56	0.0	0.0	670	-6.21	-7.52
LMC177150	M1.5 I	3600	0.77	0.0	0.0	650	-5.47	-7.26

Table 4—Continued

Star	Spectral Type	$T_{\rm eff}$	A_V	$\log g$		R/R_o[a,b]	M_V[b]	$M_{\rm bol}$[a,b]
				Model	Actual[c]			
LMC177997	M1.5 I	3675	0.77	0.0	-0.2	980	-6.71	-8.24

[a]In the case of the five stars whose $M_{\rm bol}$ found from K differ significantly from that found from V, we list both values, with the V values first.

[b]Given the 0.1 mag estimated error in $E(B-V)$, we expect that the M_V and $M_{\rm bol}$ values are determined to approximately 0.3 mag. Add to this the 50-100 K uncertainty in $T_{\rm eff}$, the uncertainty in $R/R_\odot$ is roughly 20%.

[c]Based upon adopting an approximate mass $\log(M/M_o) = 0.50 - .10M_{\rm bol}$.

Table 5. Effective Temperature Scales

Spectral Type	SMC				LMC				Milky Way			
	$T_{\rm eff}$ (K)	σ_μ[a]	N	BC$_V$	$T_{\rm eff}$ (K)	σ_μ[a]	N	BC$_V$	$T_{\rm eff}$ (K)	σ_μ[a]	N	BC$_V$
K1-K1.5 I	4211	34	7	-0.73	4300	···	1	-0.70	4100	100	3	-0.79
K2-K3 I	4025	38	15	-0.92	4050	62	3	-0.80	4015	40	7	-0.90
K5-M0 I	3788	36	10	-1.27	3850	18	2	-1.09	3840	30	3	-1.16
M0 I	3625	19	5	-1.62	3738	11	4	-1.31	3790	13	4	-1.25
M1 I	3625	···	1	-1.61	3695	8	5	-1.45	3745	17	7	-1.35
M1.5 I	···	···	···	···	3654	14	6	-1.59	3710	8	6	-1.43
M2 I	3475	···	1	-2.07	3625	7	5	-1.69	3660	7	17	-1.57
M2.5 I	···	···	···	···	3545	13	5	-1.99	3615	10	5	-1.70
M3 I	···	···	···	···	3542	18	3	-2.01	3605	4	9	-1.74
M3.5 I	···	···	···	···	···	···	···	···	3550	11	6	-1.96
M4-M4.5 I	···	···	···	···	3450	···	2	-2.18	3535	8	6	-2.03
M5 I	···	···	···	···	···	···	···	···	3450	···	1	-2.49

[a]Standard deviation of the mean.

Table 6. MARCS Galactic Bolometric Corrections[a]

$T_{\rm eff}$	BC_V	BC_K
3200	-4.58	3.16
3300	-3.66	3.08
3400	-2.81	3.00
3500	-2.18	2.92
3600	-1.75	2.84
3700	-1.45	2.76
3800	-1.23	2.68
3900	-1.06	2.61
4000	-0.92	2.53
4100	-0.79	2.47
4200	-0.70	2.40
4300	-0.61	2.33

[a]Computed for $\log g = 0.0$ models, with the zero-point defined such that $BC_V = -0.07$ for the Sun; see Bessel et al. 1998.

Appendix B

Figures

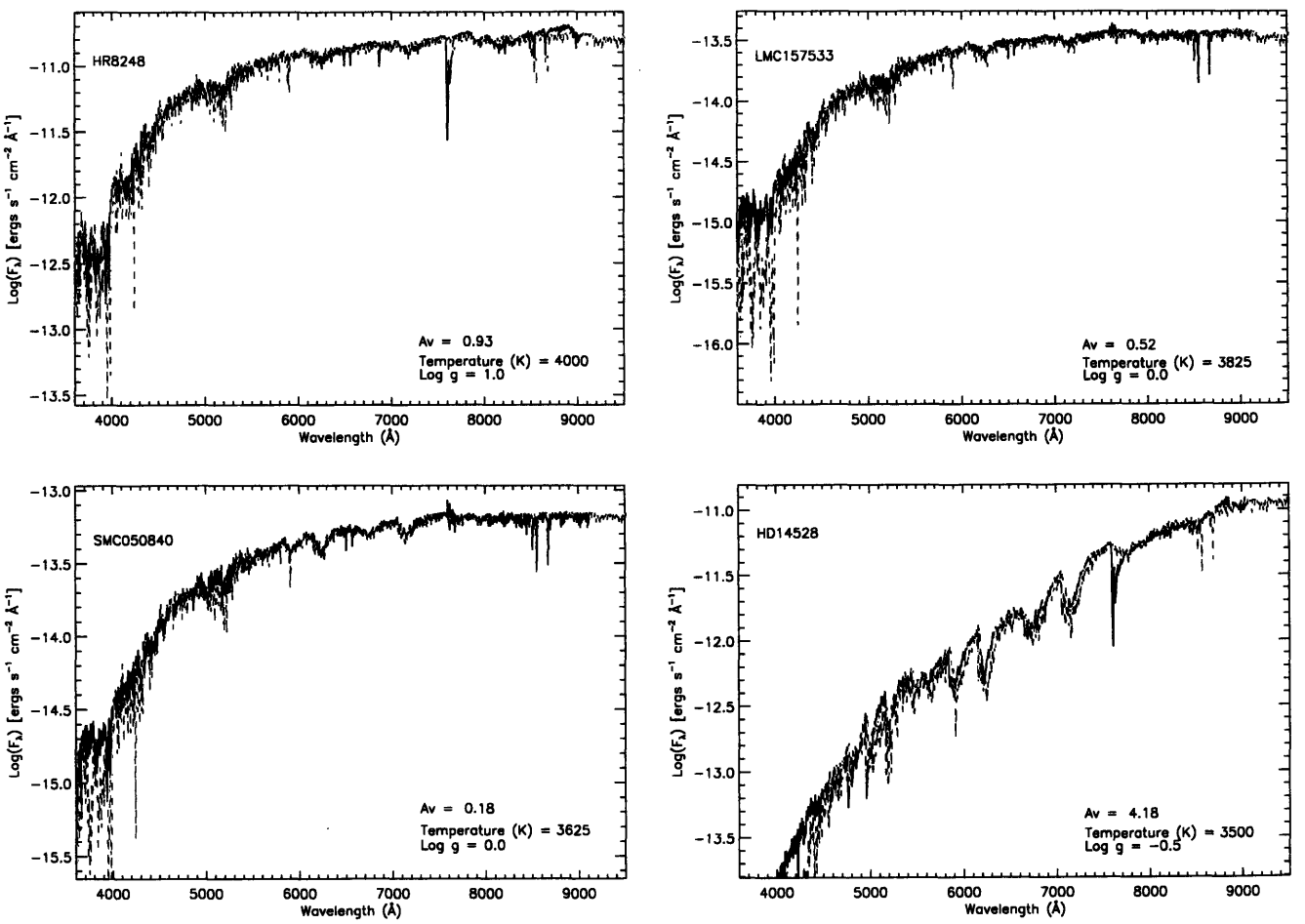

Figure B-1 **Sample SED Model Fits**
Model fits to optical spectrophotometry. Here I show examples of the fits of the MARCS models to four stars: HR 8248 (K1 I), LMC 157533 (K5 I), SMC050840 (M1 I), and HD 14528 (M4.5 I).

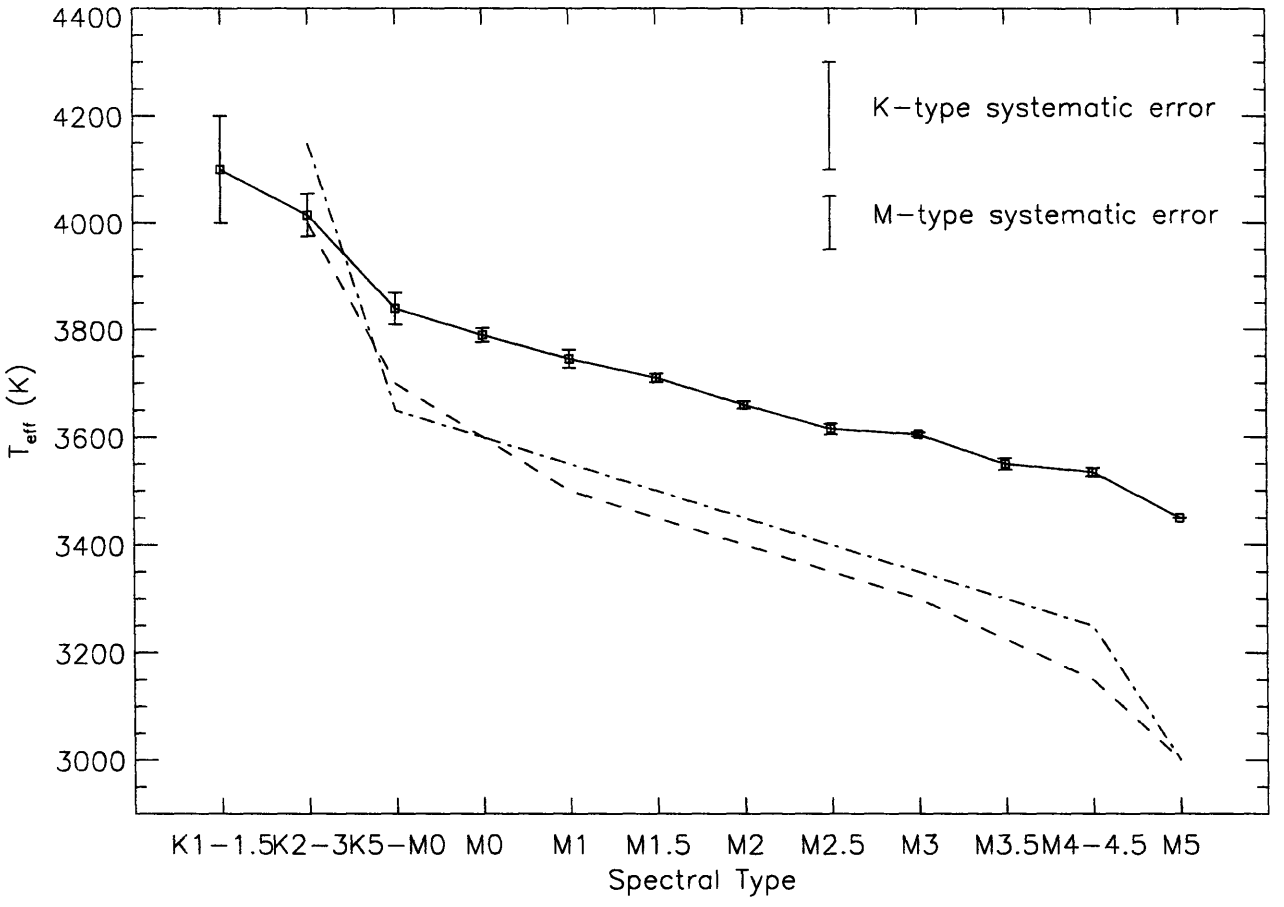

Figure B-2 **Galactic Effective Temperature Scale**
The effective temperature scale for Galactic RSGs. The error bars at each data point reflect the standard deviation of the means from Table 5, and the errors bars at the upper right show the systematic error for different spectral types. For comparison, I show the scales of Humphreys & McElroy (1984) (dashed line) and Massey & Olsen (2003) (dash-dotted line).

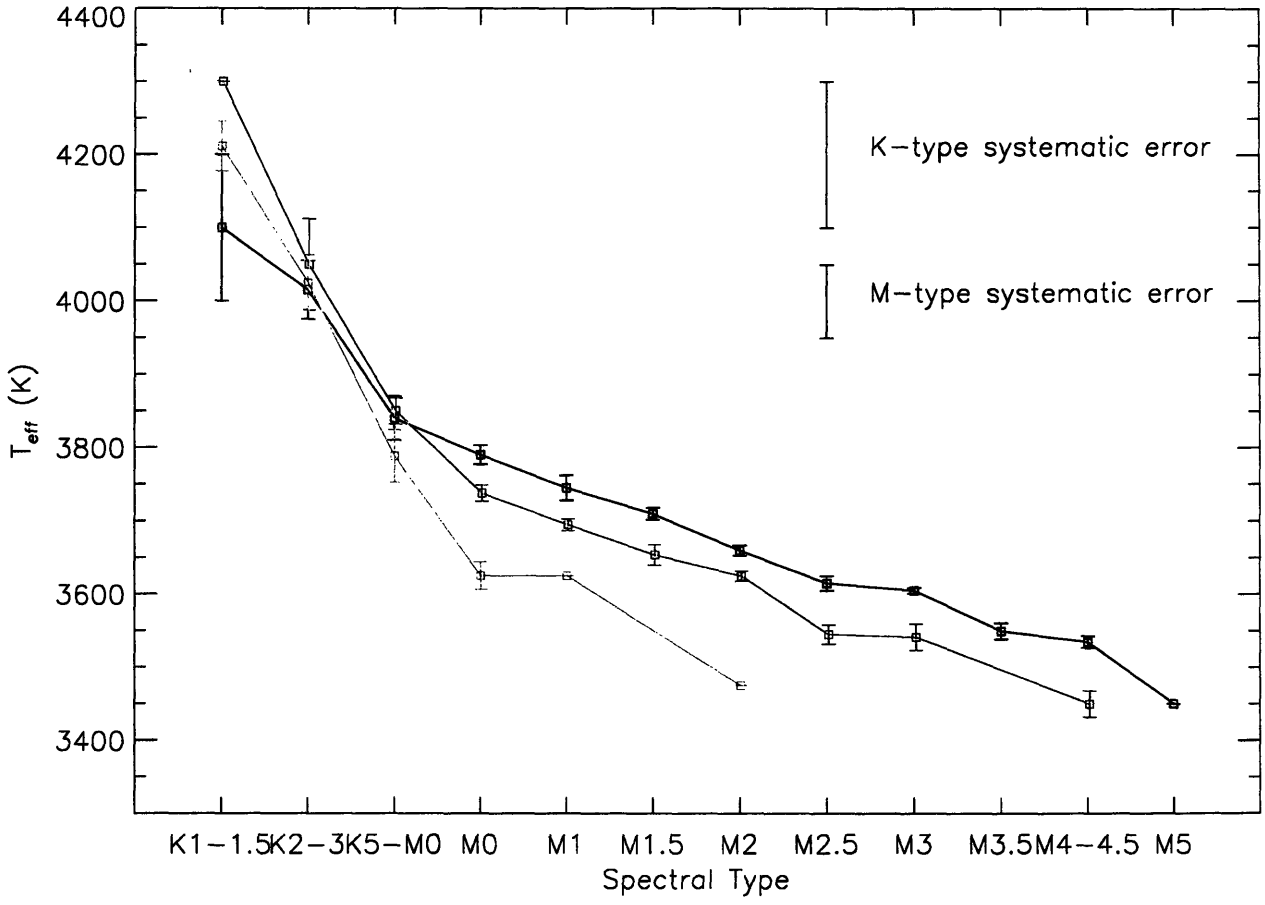

Figure B-3 **Comparison of Effective Temperature Scales**
Effective temperature scales for Galactic (black), LMC (red), and SMC (green) RSGs. The error bars at each data point reflect the standard deviation of the means from Table 5, and the errors bars at the upper right show the systematic error for different spectral types.

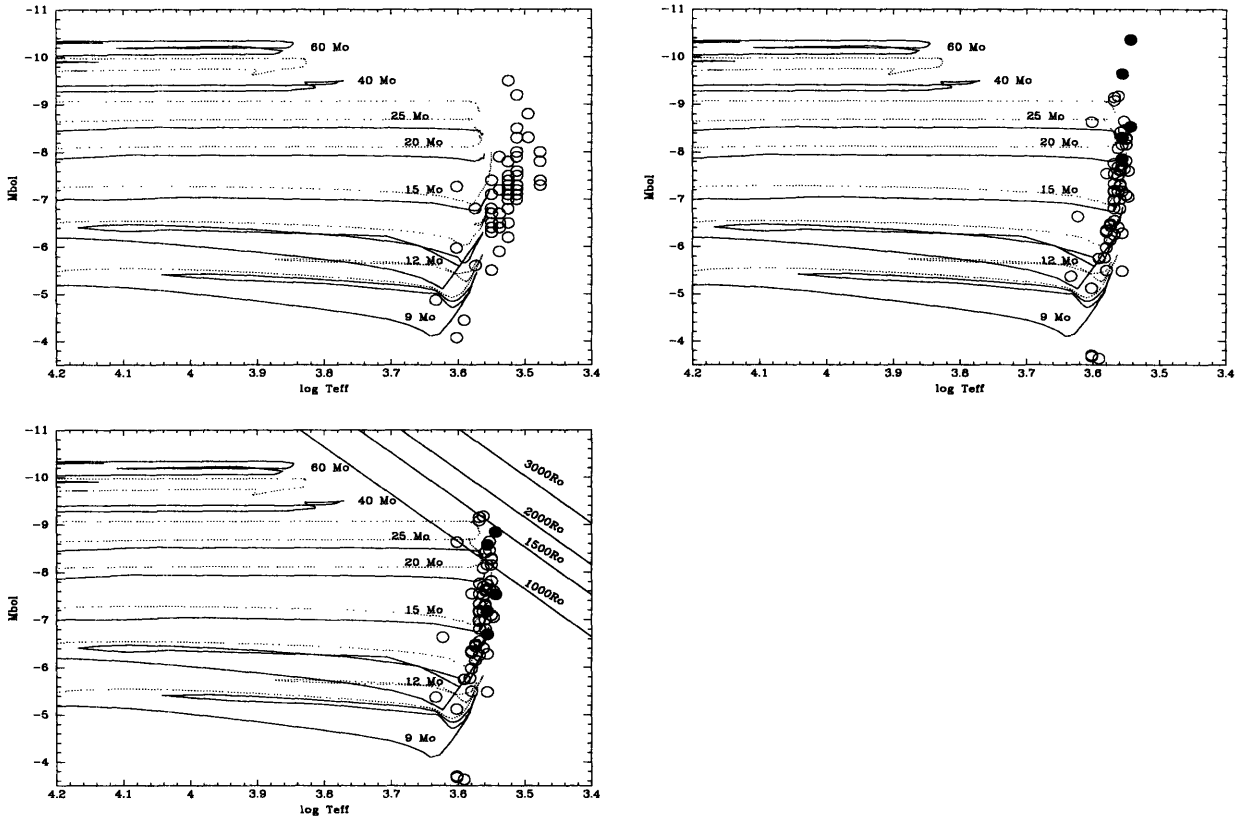

Figure B-4 **Comparison with Galactic Evolutionary Tracks**
The evolutionary tracks of Meynet & Maeder (2003) are shown, along with the location of Galactic RSGs. The solid lines denote the no-rotation models, while the dotted lines show the evolutionary tracks for an initial rotation velocity of 300 km s^{-1}. The tracks with rotation appear above the no-rotation tracks; the one for 60 $M_{\odot}$ does not extend this far to the right in the HRD. In the top left panel I show the location of the RSGs taken from Humphreys (1978), using the effective temperature and bolometric corrections of Humphreys & McElroy (1984). In the top right panel I show the location of the RSGs using our new model fits (from Table 4). The filled circles in the upper right and lower left panels denote those five stars whose luminosities derived from V are significantly higher than those derived from K. In the bottom left panel I show these same five stars with the luminosities derived from K. The diagonal lines at upper right in this figure show lines of constant radii.

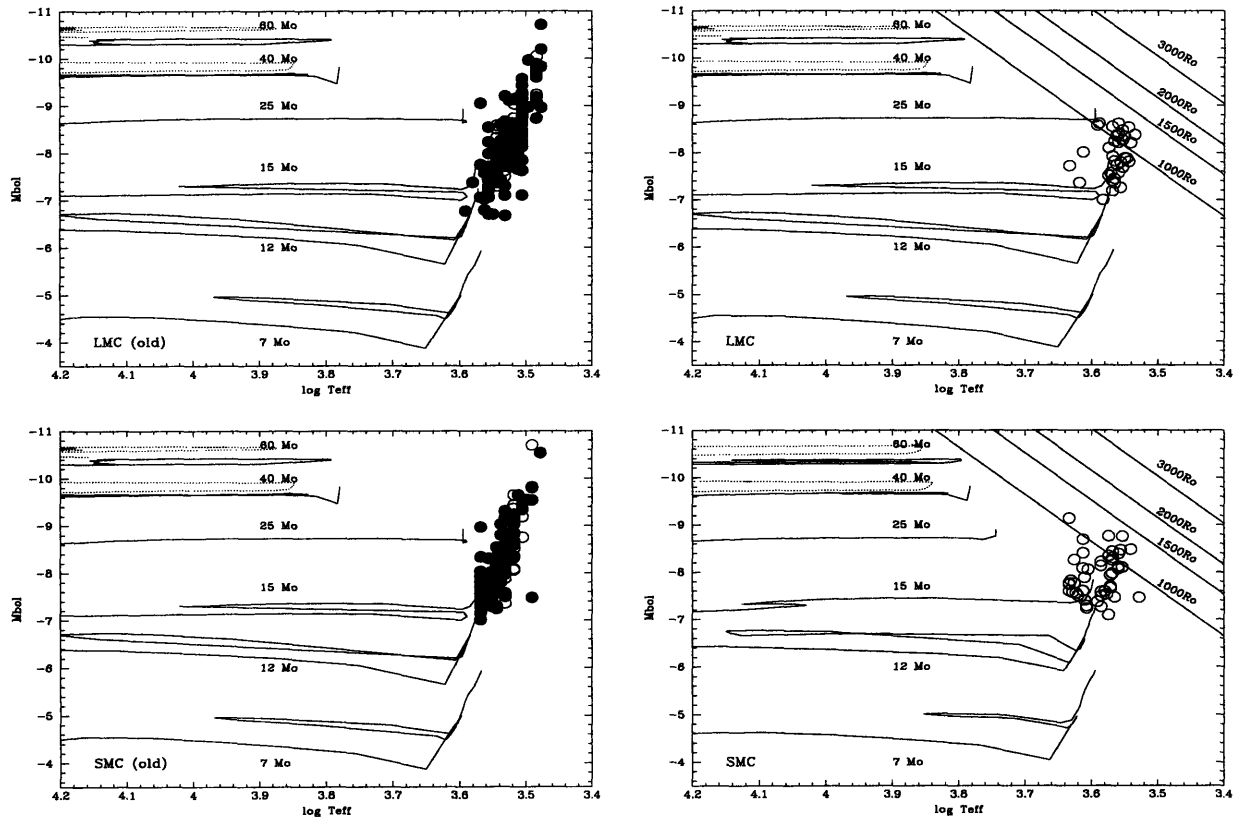

Figure B-5 **Comparison with Magellanic Cloud Evolutionary Clouds**
The location of Magellanic Cloud RSGs compared to the evolutionary tracks. In the two top panels I show the location of the LMC RSGs in the H-R diagram from the literature (left) and from fitting the MARCS models to the optical spectrophotometry (right). In the two lower panels I show the location of the SMC RSGs in the H-R diagram from the literature (left) and from fitting the MARCS models (right). The evolutionary tracks are from Charbonnel et al. (1993) for the SMC and Schaerer et al. (1993) for the LMC. The dotted lines for the 40 R_{solar} and 60 R_{solar} tracks show the effects of the newer opacities and an initial rotational velocity of 300 km s^{-1} (Meynet & Maeder 2005). The diagonal lines at upper right in these figures show lines of constant radii.